JACS
JOURNAL OF THE AMERICAN CHEMICAL SOCIETY
Article
Cite This: J. Am. Chem. Soc. 2018, 140, 7510−7518
pubs.acs.org/JACS

High-Throughput Density Measurement Using Magnetic Levitation

Shencheng Ge,[†] Yunzhe Wang,[†] Nicolas J. Deshler,[†] Daniel J. Preston,[†] and George M. Whitesides*[,†,‡,§]

[†]Department of Chemistry & Chemical Biology, Harvard University, 12 Oxford Street, Cambridge, Massachusetts 02138, United States

[‡]Wyss Institute for Biologically Inspired Engineering, Harvard University, 60 Oxford Street, Cambridge, Massachusetts 02138, United States

[§]Kavli Institute for Bionano Science & Technology, Harvard University, 29 Oxford Street Cambridge, Massachusetts 02138, United States

Supporting Information

ABSTRACT: This work describes the development of an integrated analytical system that enables high-throughput density measurements of diamagnetic particles (including cells) using magnetic levitation (MagLev), 96-well plates, and a flatbed scanner. MagLev is a simple and useful technique with which to carry out density-based analysis and separation of a broad range of diamagnetic materials with different physical forms (e.g., liquids, solids, gels, pastes, gums, etc.); one major limitation, however, is the capacity to perform high-throughput density measurements. This work addresses this limitation by (i) re-engineering the shape of the magnetic fields so that the MagLev system is compatible with 96-well plates, and (ii) integrating a flatbed scanner (and simple optical components) to carry out imaging of the samples that levitate in the system. The resulting system is compatible with both biological samples (human erythrocytes) and nonbiological samples (simple liquids and solids, such as 3-chlorotoluene, cholesterol crystals, glass beads, copper powder, and polymer beads). The high-throughput capacity of this integrated MagLev system will enable new applications in chemistry (e.g., analysis and separation of materials) and biochemistry (e.g., cellular responses under environmental stresses) in a simple and label-free format on the basis of a universal property of all matter, i.e., density.

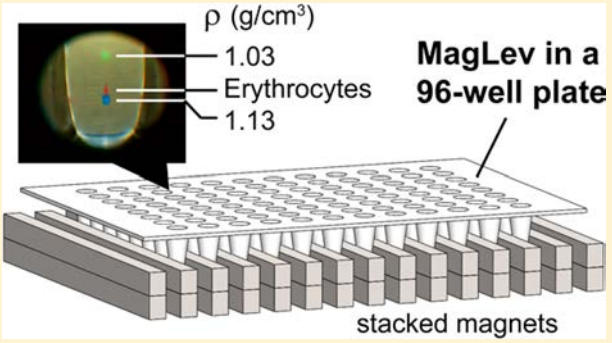

INTRODUCTION

Density is a fundamental physical property of all matter: the density of homogeneous matter (solids, liquids, gels, or gases) is simply described by the ratio of mass to volume ($\rho = m/V$). Heterogeneous matter (composites, polymers with amorphous and crystalline regions, or phase-separated regions) has a density averaged over the volumes of the different subregions described by the same formula, since these regional densities may differ. Changes in density are associated with changes in both physical and chemical properties of a material. (For example, the densities of polymers, such as solid plastic parts, may depend on their method of fabrication, or following chemical degradation when they are exposed to UV irradiation or acids/bases.[1]) Cells of different types have different densities. (For example, the densities of erythrocytes are different than the densities of adipocytes rich in fat, and even than sickled erythrocytes.[2])

Density is broadly useful to separate, characterize, and/or identify both biological and nonbiological materials. Density-based methods have been used routinely to characterize materials, to separate, isolate, or fractionate subpopulations from complex mixtures, and to follow changes in density in a wide range of systems (e.g., responses of biological cells to drug treatments, such as bacteria,[3] and chemical reactions, such as polymerization[4]).

Existing analytical methodologies, from simple centrifugation-based methods (e.g., Percoll gradient centrifugation) to more specialized techniques and types of instrumentation (e.g., methods based on pycnometers, density gradient columns, or vibrating tube densitometers), are important routine methods.[5] More complex approaches (e.g., microfluidics-based approaches using cantilever-based microresonators)[6] are also expanding the uses of density.

We also recently developed two distinct but complementary approaches to perform density measurements and/or separations: (i) One is based on the use of aqueous multiphase polymer systems (AMPS), mixtures of polymers that form distinct phases with different densities in water.[7] These phases are separated by interfaces that are sharp on the molecular scale; these phases and interfaces can be used to perform density-based separations.[8] (ii) The second is magnetic levitation (MagLev), a technique that uses competing gravitational (buoyant) and magnetic forces to form an effectively

Received: February 1, 2018
Published: June 11, 2018

DOI: 10.1021/jacs.8b01283
J. Am. Chem. Soc. 2018, 140, 7510−7518

continuous density gradient in an aqueous paramagnetic medium in a magnetic field, and allows separations of particles suspended in the medium on the basis of their densities.[9] MagLev using permanent magnets and paramagnetic media, as we have been developing it, is a versatile tool for measurement of density.[9] It is broadly applicable to a wide variety of samples.[9]

The device most commonly used for MagLev (Figure 1) consists of two NdFeB permanent magnets placed coaxially

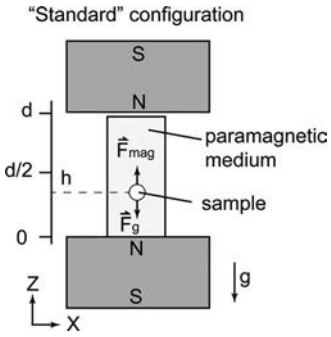

Figure 1. Overview of MagLev. In the "standard" configuration of MagLev, a sample levitates stably at a distance of h to the bottom magnet when the gravitational force ($\vec{F}_g$, corrected for the effect of the buoyancy) acting on the sample balances the magnetic force ($\vec{F}_{mag}$, as a result of direct interaction of the magnetic field and the paramagnetic medium that surrounds the sample).

with like-poles facing, and uses a cuvette filled with a paramagnetic medium as the container to levitate samples (when placed between the two magnets).[10,11] (MagLev is distinct from the magnetic separation technologies common in biochemistry, which use superparamagnetic particles and involve magnetic fields to separate these particles from diamagnetic suspensions.[12−14]) The central axis of the MagLev device is aligned with the gravitational field, and the objects levitate vertically along this axis. In this configuration, MagLev covers a density range of ∼0.8 to ∼3 g/cm^3 when the paramagnetic solution is a concentrated solution of common paramagnetic salts such as $MnCl_2$ and $GdCl_3$.[9] Depending on the dimensions and orientation of the magnets, the metrics for analytical performance (primarily dynamic range and sensitivity) can be appropriately optimized to cover the entire range of densities (∼0 to ∼23 g/cm^3) observed in matter at ambient temperature,[15] or reach an exceptionally high sensitivity, up to ∼10^{-6} g/cm^3, in resolving differences in density.[16] Demirci and Tasoglu have miniaturized this "standard" MagLev device and demonstrated its application in the measurements of densities of single cells.[3,17] The "standard" MagLev device and its variants, however, are limited to measurement of one sample (which may, nonetheless, comprise a number of different sample components) at a time, and therefore, are not directly useful for high-throughput measurements.

This paper describes an integrated analytical system using MagLev that makes it possible to carry out density-based array screening. This system integrates a flatbed scanner and simple optical components (mirrors and lenses) to acquire images of the levitated contents (often in the form of particles) in aqueous paramagnetic media (with a working volume of ∼50 μL per sample) in a 96-well plate format.

We engineered a magnetic field between two pairs of like-poles facing, stacked magnets (see Figures 1−3 for details) to

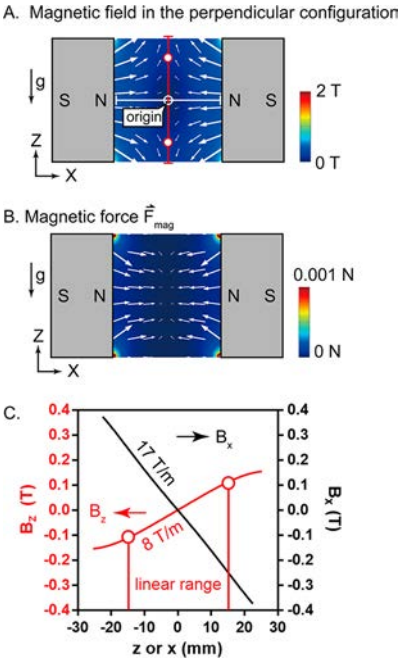

Figure 2. Magnets, fields involved in MagLev as described in this study. (A) In the perpendicular "standard" configuration, the gradient in magnetic field is parallel to the surfaces of the magnets (red solid line), rather than perpendicular to the surfaces of the magnets (white solid line); this "parallel" configuration is also aligned with the gradient due to gravity. The pair of open circles mark the approximately linear range of the gradient. (B) Magnetic force (estimated using eq 1 and plotted as $2.3\log|\vec{F}_{mag}|$) that a diamagnetic particle (5 mm in diameter, modeled after the commonly used density standard beads) experiences when it is suspended in an aqueous solution of 1 M $MnCl_2$, and placed in the field between the magnets. (C) Strength of the magnetic field along the red and white lines in (A).

levitate multiple samples in a paramagnetic medium. We took advantage of the magnetic gradient along the vertical centerline in the gap between the faces of the magnets and made an array of these gradients in space so that the device is compatible with one of the most common types of containers for arrays of small (up to ∼300 μL) liquid samples in the laboratory, a 96-well plate.

This format used long and thin magnets ($L \times W \times H$ for each indistinguishable magnet: 101.6 mm × 4.8 mm × 6.4 mm). These magnets were inserted in the spaces between the rows of tubes on a 96-well plate with the like-poles facing one another. This format allows parallel reading using indistinguishable (in principle) magnetic fields around each well.

Finite-element simulation in COMSOL evaluated the profile of the magnetic field in the gaps of the magnet array. The dimensions used for the array generated both a strong magnetic field (up to ∼0.7 T along the central z-axis in the gaps) and field gradient, and therefore, required low concentrations of paramagnetic salts to levitate samples (e.g., ∼0.5 M $MnCl_2$ covers a range of densities from ∼1.0 g/cm^3 to ∼1.6 g/cm^3, which would otherwise require ∼3 M $MnCl_2$ to cover the same range in the "standard" MagLev device[9]). Low concentrations of paramagnetic salts improve the biocompatibility of the suspending media, and are particularly useful for levitating biological cells.

Parallel density measurements across the entire 96-well plate validated the performance of the system—and particularly its reproducibility. We demonstrated broad applicability of high-

DOI: 10.1021/jacs.8b01283
J. Am. Chem. Soc. 2018, 140, 7510−7518

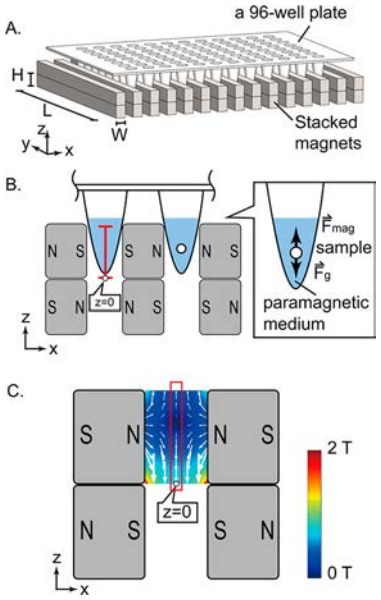

Figure 3. Array of magnets designed for high-throughput density measurements. (A) Magnets (15 pairs in total, L × W × H for each magnet is 101.6 mm × 4.8 mm × 6.4 mm) are evenly spaced (the width of the gap is 4.2 mm) with the like-poles facing one another, and 11 of these pairs are positioned in the space between the rows of the tubes on a 96-well plate. The dimensions of the magnets are based largely on the dimensions of those commercially available. (B) The red line indicates the magnetic field we exploited to levitate samples in this configuration. A sample levitates in a paramagnetic medium when the gravitational force F_g (corrected for the effect of buoyancy) acting on the sample balances the magnetic force F_{mag}, which the sample experiences as a result of direct interaction of the magnetic field and the paramagnetic medium that surrounds the sample. (C) Simulation using COMSOL shows the cross-sectional profile (on the $x-z$ plane) of the magnetic field in the gap between a pair of magnets in (A). The red box highlights the field that we exploited in this study.

throughput density measurements of biological and non-biological materials in aqueous paramagnetic media using this MagLev-based system for three representative types of samples: (i) surfactant-stabilized drops of 3-chlorotoluene (a hydrophobic liquid), (ii) small solid particles and powders (crystals of cholesterol, glass particles, copper powder, and polymer beads), and (iii) human erythrocytes.

MagLev has eight important characteristics that make it useful in performing high-throughput density measurements: (i) MagLev is simple in design and use. It uses permanent magnets to generate a magnetic field, and does not require electricity to operate (though the scanner we used to image the device requires electrical power). The device can be assembled simply, and be used, in principle, indefinitely without maintenance beyond occasional calibration. (ii) MagLev usually uses inexpensive, commercially available paramagnetic salts (especially $MnCl_2$) to generate appropriate media in aqueous solutions. ($DyCl_3$ is also sometimes particularly useful for its high magnetic susceptibility.[18]) (iii) MagLev is a label-free method that directly measures the densities of the materials. It does not require chemical derivatization or labeling (e.g., with chromophores or fluorophores). (iv) It can be used in a format that enables parallel measurements and, thus, the ability to do high-throughput measurements of density (this paper). (v) MagLev as we describe here covers a wide range of densities, from an air bubble (~0 g/cm^3, using 3 M $DyCl_3$, data not shown) to copper particles (8.96 g/cm^3), and has a tunable sensitivity in density measurements (this study demonstrated $\Delta\rho$ as small as ~0.001 g/cm^3 using 0.1 M $MnCl_2$). (vi) MagLev requires only small quantities of samples. (It can easily detect single colored particles ~200 μm in diameter.) It can be applied to a variety of samples with different physical forms (e.g., heterogeneous, sticky, fragile, and/or irregularly-shaped samples). (vii) MagLev enables measurements over a convenient interval of time (typically a few minutes to <1 h for a single scan of the plate). (viii) The configuration of MagLev we describe here is compatible with a simple flatbed scanner for imaging purposes.

The major limitations of the system we describe include (i) inability to measure densities of samples having a large size (e.g., mm or above), and (ii) requirement of paramagnetic media that do not dissolve (or react with) the materials of the plates or the sample. (This study used plates made of polypropylene.)

The ability of high-throughput density measurements using MagLev will, as in other areas of analytical chemistry and biochemistry, generate new applications. In particular, the simplicity and affordability of the system expands the range of applications for which it might be used.

EXPERIMENTAL DESIGN

Theory of MagLev. Previous papers have described the theory of MagLev,[9,15,16] and the description below includes only an overview of the "standard" MagLev device and the key equations used to guide the design of the current, "parallel" MagLev device.

The "standard" MagLev device (Figure 1) comprises two NdFeB permanent magnets positioned with the like-poles facing ($L \times W \times H$ for each indistinguishable magnet: 50.8 mm × 50.8 mm × 25.4 mm) and coaxially at a distance of 45.0 mm to yield an approximately linear magnetic field along the central axis between the magnets. This central axis aligns with the vector of gravity. When a diamagnetic sample is placed in a container filled with a paramagnetic medium and then centered coaxially in the device, the sample can float, or levitate, stably without physically contacting the container. At equilibrium, the gravitational force $\vec{F}_g$ acting on the object (corrected for the effect of buoyancy) balances the magnetic force $\vec{F}_{mag}$, the physical force the sample experiences as a result of the direct interaction of the magnetic field and the paramagnetic medium that surrounds the sample. The levitation height h, the distance from the centroid (the geometric center) of the sample to the top surface of the bottom magnet, is proportional to the density of the sample, and therefore, can be measured experimentally (with appropriate calibrations using known density standards) to calculate the unknown density of the sample.

Equation 1 describes the balance of physical forces acting on the levitated sample. Equation 2 shows that the density of the sample that levitates at a given position can be calculated (to a good approximation) using the characteristics of the suspending medium (including its density, ρ_m, and magnetic susceptibility, χ_m), the magnetic susceptibility of the sample, χ_s (which is usually negligible in comparison to χ_m),[9] and the strength and gradient of the magnetic field $B_z(dB_z/dz)$ at the position of equilibrium.

$$\vec{F}_g + \vec{F}_{mag} = (\rho_s - \rho_m)V\vec{g} + \frac{(\chi_s - \chi_m)}{\mu_o}V(\vec{B}\cdot\vec{\nabla})\vec{B} = 0 \quad (1)$$

$$\rho_s \approx \frac{(\chi_s - \chi_m)}{\mu_o g}\left(B_z\frac{dB_z}{dz}\right) + \rho_m \quad (2)$$

In eqs 1 and 2, $\vec{F}_g$ (N) is the gravitational force corrected for the effect of buoyancy, $\vec{F}_{mag}$ (N) is the magnetic force, ρ_s (g/cm^3) is the density of the suspended sample, ρ_m (g/cm^3) is the density of the paramagnetic medium, $\vec{g}$ (−9.810 m/s^2) is the vector of gravity, χ_m (unitless) is the magnetic susceptibility of the paramagnetic medium,

DOI: 10.1021/jacs.8b01283
J. Am. Chem. Soc. 2018, 140, 7510−7518

χ_s (unitless) is the magnetic susceptibility of the suspended sample, μ_o ($4\pi \times 10^{-7}$ N/A^2) is the magnetic permeability of free space, V (m^3) is the volume of the object, $\vec{B}$ (T) is the magnetic field, $\vec{\nabla}$ is the gradient operator, B_z is the z-component of the magnetic field, and (dB_z/dz) is the gradient of the z-component of the field along the central z-axis.

This work exploited the magnetic field gradient that is *perpendicular* to the central z-axis of the "standard" configuration, and aligned it to the gravity, to levitate samples suspended in paramagnetic media (Figure 2A). To illustrate this design, we rotated the "standard" configuration 90° in the $x-z$ plane about the geometric center. The field gradient exploited in the "standard" configuration now became horizontal (the solid white line, Figure 2A); the field gradient exploited in this study (highlighted by the solid red line, Figure 2A) became aligned with that of gravity. (The force of gravity is constant across the sample.) The linear range of this gradient (bounded by the open red circles, Figure 2A) is functionally similar to the gradient along the central axis in the "standard" configuration for levitating samples in paramagnetic media (against gravity). When a sample is suspended in a paramagnetic medium and then placed in this magnetic field, the sample will experience a magnetic force that pushes it toward the central z-axis, and simultaneously reach its position of equilibrium along the z-axis based on the balance of physical forces along this axis (eq 1). Equations 1 and 2 are equally applicable to the samples that levitate in the linear range of the field (B_z, Figure 2C, which is slightly weaker than the gradient we exploited in the "standard" configuration, B_x).

Design of the Magnet Array. Inserting magnets into the space between rows of tubes along the shorter dimension of the 96-well plate established the magnetic field for the tubes (Figure 3A). The profile of the magnetic field between every pair of like-poles facing magnets (i.e., N/N or S/S) is similar to that in the "standard" single-sample, MagLev device. We took advantage of the vertical field gradient (i.e., along the z-axis, Figure 2A, solid red line) in parallel to the faces of the magnets to levitate samples suspended in a 96-well plate.

We also wished to develop this configuration of MagLev so that it would be compatible with biological samples. Two different but complementary approaches increased the strength and gradient of the magnetic field (Figure 3B, solid red line) and, thus, minimized the concentrations of paramagnetic salt used to levitate living cells and other samples sensitive to high concentrations of salts (eq 2). (i) Decreasing the size of the magnets relative to those we used in the "standard" configuration was a natural step in designing the magnet array to be compatible with the 96-well plate. The spatial profiles of the magnetic fields for permanent magnets (single or combinations) are uniformly scalable—that is, the shape and strength of the magnetic field are maintained as the absolute dimension of the field changes (e.g., compare the values of gradients in Figure 2C vs Figure 4B).[19] This miniaturization, therefore, allows straightforward adjustment of the gradient of the magnetic field. (ii) Stacking an additional set of magnets at the bottom of the first set (Figure 4) enhanced the strength of the magnetic field in the gaps of the array. This approach of simple stacking of magnets increased the gradient of the field (from 137 T/m to 198 T/m, a factor of ~1.45, Figure 4B), and also increased the value of $B_z(dB_z/dz)$ (e.g., from 28 T^2/m to 116 T^2/m at z = 1.5 mm, a factor of 4.14, Figure 4C). The strength of the gradient is critical in determining the concentration of paramagnetic species required to levitate a sample of a given density (eq 2). See Figures S1 and S2 for details on simulation of the magnetic fields (using Comsol).

Choice of Paramagnetic Medium. MagLev, as used here, requires a paramagnetic medium to levitate a diamagnetic sample. In addition, the paramagnetic medium should be compatible with (e.g., unreactive with, nondissolving, nontoxic toward) the sample to be levitated. Cost, commercial availability, volatility, and density are also important. For biological samples, only water is relevant as a solvent.

For nonbiological applications, simple paramagnetic salts (e.g., aqueous solutions of $MnCl_2$ or $GdCl_3$), hydrophobic Gd chelates (dissolved in hydrophobic solvents, such as aromatic hydrocarbons), and also paramagnetic ionic liquids can be used to levitate objects.[9,20,21]

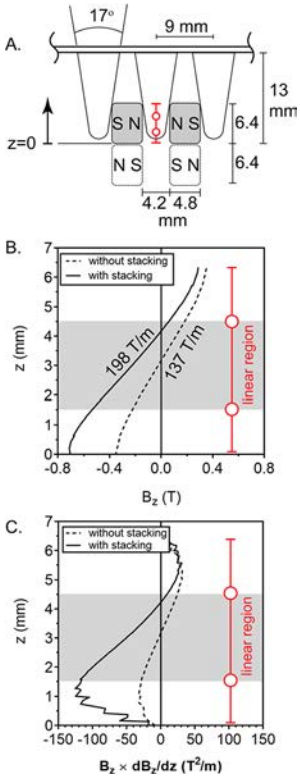

Figure 4. Magnetic field strength in the gaps of the magnet array. (A) Schematic shows the key dimensions of a 96-well plate used in this study, and the spatial arrangement and dimensions of the magnets between the tubes. The red line indicates the magnetic field that levitates samples, and the pair of open circles mark the linear region. (B) The magnitude of B_z along the central z-axis in the gap increased by stacking a second set of magnets (represented by the white boxes in A) below the first set (represented by the filled boxes in A). The equations of linear fits to the curves within the highlighted region are $z = 5.06B_z+4.18$ ($R^2 > 0.99$, solid curve) and $z = 7.34B_z+3.18$ ($R^2 > 0.99$, dashed line). (C) The magnitude of $B_z(dB_z/dz)$ increased by ~4× at z = 1.5 mm by stacking a second set of magnets. The jagged steps on the lines are due to the low spatial resolution we used in the simulation.

For biological applications, we previously have used biologically compatible Gd·DTPA (Gd^{3+} chelated with diethylenetriaminepentaacetic acid) to magnetically trap and translate single cells in 3D.[22] Others have used similar Gd chelates, such as gadobutrol (Gadovist) and gadobenate dimeglumine (MultiHance), to levitate living cells for separations and analyses.[3,23] This paper used gadobutrol to levitate living cells because of its excellent biological compatibility, based on preliminary work with cells. Given the commercial availability of a large range of paramagnetic chelates (e.g., based on Gd^{3+} or Mn^{2+}), and differences in cost and performance, selection of chelates for specific applications should be evaluated where appropriate.

Design of an Apparatus, Incorporating a Flatbed Scanner, to Image Samples That Levitate in a 96-Well Plate. A flatbed scanner provided a simple, affordable imaging device to acquire images of levitated samples in a 96-well plate. A specific model (Perfection V550 from Epson) has six useful characteristics: (i) It is inexpensive (~$200 for one scanner) and requires (in our experience) minimal maintenance. (ii) The imaging area of the scanner is large (216 mm × 297 mm) and can accommodate up to two 96-well plates (80 mm × 120 mm) positioned end-to-end with the long axis of the plate parallel to the centerline of the scanner. (iii) This model has a built-in light source: an LED that provides a uniform, line illumination. It is used in the "transmittance" mode to scan transparency films, and has a width (~83 mm, perpendicular to the direction of scanning) that can span the full width of a 96-well plate (80 mm). The lid is also detachable

DOI: 10.1021/jacs.8b01283
J. Am. Chem. Soc. 2018, 140, 7510−7518

from the scanner body, and thus, can be raised in height to accommodate the MagLev device (Figure S7). (iv) The scanner has a high optical resolution (6400 dpi, i.e., ∼4.0 μm per dot), a resolution useful to image small particles (e.g., suspended powders or clusters of cells). (v) The scanning process is fast (e.g., it took ∼10 min to scan an entire 96-well plate at a resolution of 6400 dpi). (vi) The scanner is compact, lightweight, and easily portable.

One major shortcoming in directly using the flatbed scanner to image levitated samples in the MagLev device is that the scanner has its focal plane at the flatbed, and has a limited depth of field to resolve clearly samples that are placed at a distance above the focal plane, or the flatbed. For the configuration of the MagLev device we describe in this work, we inserted mirrors in the gaps of the magnet array and between the tubes, the only space we can conveniently access to install mirrors for the tubes at ∼45° to project images of the tubes downward to the scanner. The images of the samples in the mirrors that formed are at least ∼13 mm (the height of the stacked magnets) above the flatbed of the scanner.

To solve this "out-of-focus" problem, we employed an array of relay lenses, a lens (e.g., a simple, inexpensive, biconvex plastic lens) that would form a focused image of an object on the other side of the lens, to project focused images of the samples within the tubes onto the flatbed of the scanner, the plane on which we usually place samples (e.g., a document) to be scanned.

In addition, the specific design of the scanner using a single focusing lens (or equivalent) has an oblique angle in viewing a 3D object placed on the flatbed, in a position that is laterally shifted from its central axis (*c*-axis, Figure 5; see Figure S4B for an example using binder clips). Carefully adjusting the angles of the mirrors, and the lateral displacements of the lenses, D_L, with respect to the central axis of the scanner, generated focused, nonoblique views of the samples that levitated in the tubes (see Figures S3−S6 for detailed designs). Due to the particular shape of the magnetic fields between the magnets, the samples (e.g., small colored particles having the same density) levitate at the same z-coordinates, and form straight lines (in the y−z plane) parallel to the faces of the magnets (Figure 5B). Because the mirrors face the tubes in the gaps, the reflected images of the lines in the mirrors, and also the refocused images on the flatbed of the scanner, appear to the scanner as single dots (Figure 5A,B). Figure 5C shows an image of a set of four colored particles (used as density standards) that the scanner acquired. These particles appeared as single dots on the acquired image; the view to the particles behind the first particles of the same color was blocked. These particles may, however, become partially visible when they levitate at different z-coordinates due to differences in density, or slight misalignment of the mirrors and/or the lenses.

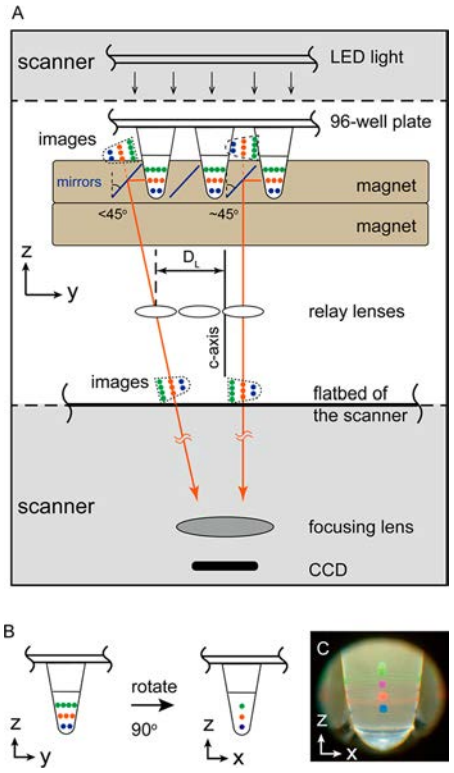

Figure 5. Imaging the samples that levitate in the tubes. (A) Spatial arrangement of the key optical components of the system. The gray regions include the key components of the scanner, and the white region sandwiched by the gray regions shows the components of the MagLev device. The *c*-axis stands for the central axis of the scanner. D_L is the lateral shift of a relay lens with respect to the *c*-axis. The direction of scanning is along the *x*-axis (perpendicular to the plane of the paper). (B) Particles having the same densities, represented by the colors, levitate at the same *z*-coordinates and form parallel lines in the tubes. These lines will appear as single dots to the scanner when the image of the tube in the mirror is refocused to the flatbed, and then to the CCD of the scanner. (C) Four density standard beads levitated at different *z*-coordinates and appeared to the scanner through the relay lens.

RESULTS AND DISCUSSION

Selecting the Number and Dimensions of Magnets. We chose a typical 96-well plate used for applications with polymerase chain reactions for this study because of the optical transparency of its thin-walled tubes, and also because it was easy to insert magnets between the rows of the tubes. We used the dimensions of the tubes that fitted in the wells (conically shaped tubes with a cone angle of ∼17°, a height of 13 mm, and an intertube spacing of 9 mm, Figure 4A) to select the number and size of the magnets.

We used COMSOL to simulate and evaluate the profile of the magnetic field in the gaps of the magnet array (Figures 3C, S1, and S2), and chose—based on the commercial availability of the magnets and the spatial constraints of the well plate—the following dimensions to construct the magnet array: 15 magnets of 101.6 mm × 4.8 mm × 6.4 mm ($L \times W \times H$). We stacked a second set of magnets of the same type at the bottom to further increase the strength of the magnetic field while maintaining an approximately linear magnetic field over ∼3 mm in the gaps (Figure 4B). The enhanced strength and gradient of the magnetic field are critical in decreasing the concentrations of the paramagnetic salts required to levitate living cells.

Preparing Density Standards. We usually use commercially available and highly precise (±0.0002 g/cm^3) density standards (glass beads, American Density Materials, Inc.) to calibrate the "standard" MagLev device. These beads are ∼4−5 mm in diameter (Figure 6A), too large to be directly useful to calibrate the MagLev device we describe in this study. There are two simple methods useful to calibrate the device: (i) use small particles having known densities and (ii) use hydrophobic liquids having known densities (in the form of small droplets suspended in an aqueous solution, or emulsions). We preferred method (i) to method (ii) because multiple density standards can be easily combined in a single solution, which allows convenient preparation, use, and storage of these density standards for calibration purposes.

Density standards of small (∼200 μm in diameter), colored particles are commercially available (Cospheric, LLC); these beads, however, may have a large distribution in density (e.g., $\Delta\rho \sim 0.1$ g/cm^3 for the blue particles in Figure 6B), and thus, are suboptimal to calibrate the device we describe in this study.

DOI: 10.1021/jacs.8b01283
J. Am. Chem. Soc. 2018, 140, 7510−7518

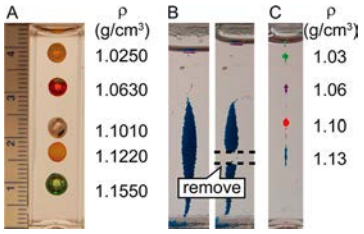

Figure 6. Preparation of density standards. (A) Set of five glass beads having precisely known densities (±0.0002 g/cm^3) levitated in an aqueous solution of 1.000 M $MnCl_2$ containing 1 wt % Tween-20 in the "standard" MagLev device. A ruler with a minimal division of 1 mm was used to measure the levitation heights, h (mm), of the beads. The calibration curve is $h = -228\rho + 273$, $R^2 > 0.99$. (B) Commercially available density standard particles (small, polyethylene-based particles) levitated under the same conditions as described in (A). We removed a small fraction by aspiration using a Pasteur pipet (indicated by the dashed lines). (C) We used the same procedure to prepare four colored density standards (including the blue particles as described in B), and determined their average densities using the centroids of the clusters and the calibration curves established in (A). These colored particles are heterogeneous in density and have a spread (~ ±0.01 g/cm^3) around their average densities.

We used the "standard" MagLev device to fractionate the beads and improve the quality of the density standards. We improved the precision in density (that is, we narrowed the distribution in density) of these beads by up to ~8×. We could, if needed, further improve the precision of the density standards using AMPS that we have described in a separate study.[24] Each population of the prepared particles has a spread in density ~ ± 0.01 g/cm^3 around its average density (Figure 6C).

Calibrations and Reproducibility across the Array. Calibration of the MagLev device used the particles prepared in 0.100 M $MnCl_2$ (Figure 7) at room temperature (23 ± 1 °C). We measured the levitation heights, defined as the apparent distance D between the centroid of the standard particle(s) and the horizontal line running through the center of the view area. (This distance D measures the separation between the centroid of the particles and the center of the viewing area on the image that formed at the flatbed, and thus, does not represent the physical distance in the tube. Figure 5.) Figure 7B shows a representative calibration curve for a tube on the plate. The linear fits of D vs density for particles that levitate in individual tubes across the plate give an excellent average R^2 of 0.97 (N = 91 wells, Figure 7C). We excluded five wells because they either missed one or more colored beads or produced low-quality images. In another set of experiments, we performed an additional calibration using small drops of anisole (ρ = 0.993 g/cm^3, stabilized by 1% Tween-20 in the suspending medium), and the combined results yielded an average R^2 of 0.98 across the plate. Together, these results validated the assumption of approximately linear magnetic fields in the magnet array.

Density Measurements of Simple Liquids and Irregularly Shaped Solids. Cholesterol and 3-chlorotoluene served as examples to illustrate the use of the MagLev device to measure the densities of simple liquids and irregularly shaped solids (Figure 8). Including 1% surfactant Tween-20 in the suspending medium (0.100 M $MnCl_2$) facilitated the dispersion of the hydrophobic compounds (particles or liquid drops) in the aqueous suspending medium. At equilibrium, the small drops of 3-chlorotoluene appeared as white clusters in the

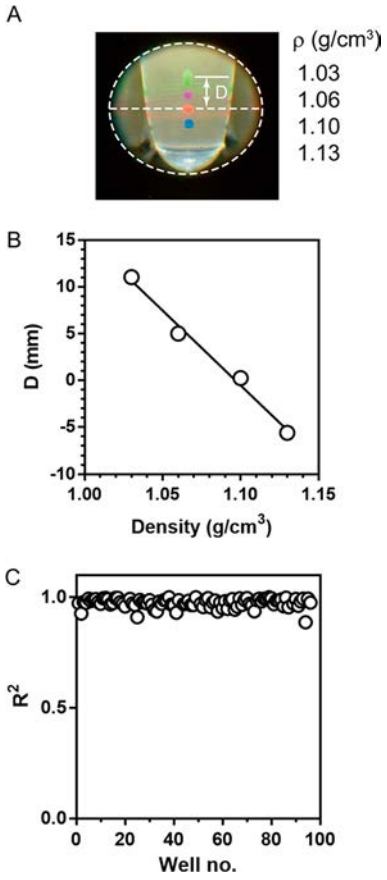

Figure 7. Calibration of the MagLev device. (A) Four colored density standards levitated (in 0.100 M $MnCl_2$ with 1% Tween-20 to facilitate the dispersion of these hydrophobic particles) at different distances to the center of the viewing circle. The distance D is defined as the apparent distance between the centroid of the particles and the center of the viewing circle on the image (highlighted by the dashed lines). To convert the number of pixels to the distance D, we imaged a ruler with mm markings (placed on the flatbed of the scanner) and used it to calculate the conversion. (B) Representative plot of D vs the densities of the particle(s) in a single tube. $D = -160(\pm 12)\rho + 176(\pm 13)$, $R^2 = 0.99$. The values for the slope and the intercept are presented as best-fit value ± SD of the best-fit value. (C) Coefficient of determination R^2, or the goodness of the linear fit of D vs density for the standard particles in each well, across the plate. N = 91 wells.

tubes. We determined the centroids of the clusters, and estimated the densities independently for each tube using the calibration curve established for that tube (e.g., the equation described in the caption of Figure 7B). A representative value of density is estimated to be 1.068 ± 0.006 g/cm^3 (mean ± estimated SD, N = 1 well, see the Supporting Information). We also took advantage of the parallel measurements, and combined all the individual measurements to yield an estimated density of 3-chlorotoluene, 1.069 ± 0.008 g/cm^3 (mean ± SD, N = 95 wells). This estimate agrees ($\Delta\rho$ is 0.006 g/cm^3) with the reported value, 1.075 g/cm^3.[25] Similar calculations for the sample of cholesterol yielded an estimated density of 1.030 ± 0.005 g/cm^3 (mean ± SD, N = 95 wells); this estimate agrees reasonably well ($\Delta\rho$ is 0.037 g/cm^3, or ~4%) with the reported value, 1.067 g/cm^3.[25] (The low value may reflect small air bubbles trapped in the irregularly shaped particles. We did not degas the sample to test this possibility.)

Separation and Density Measurements of Mixtures of Particles and Powders. A mixture of spherical glass particles

DOI: 10.1021/jacs.8b01283
J. Am. Chem. Soc. 2018, 140, 7510−7518

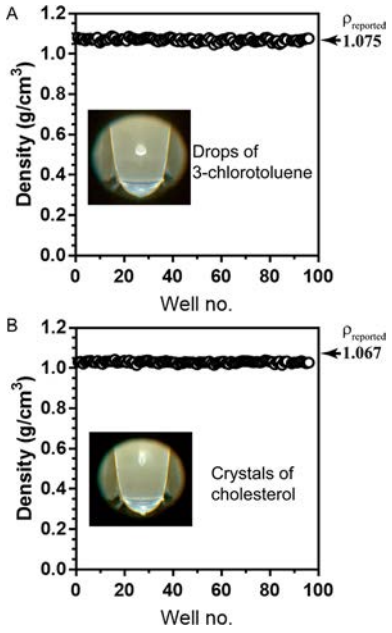

Figure 8. Density measurements of a liquid and a solid. (A) We levitated small, surfactant-stabilized droplets of 3-chlorotoluene in an aqueous solution of 0.100 M $MnCl_2$. The sample was prepared by vigorously shaking 0.5 mL of 3-chlorotoluene in 20 mL of $MnCl_2$ solution containing 1 wt % Tween-20, and adding the sample as an emulsion to the wells using a 12-channel pipettor. The estimated density of 3-chlorotoluene is 1.069 ± 0.008 g/cm^3 (N = 95 wells). The literature value ($\rho_{reported}$ = 1.075 g/cm^3) was included for comparison. (B) Small crystals of cholesterol, in an aqueous solution of 0.100 M $MnCl_2$, yielded an estimated density of cholesterol, 1.030 ± 0.005 g/cm^3 (N = 95 wells). The literature value ($\rho_{reported}$ = 1.067 g/cm^3) was included for comparison.

and irregularly shaped copper powder was prepared as an example to demonstrate the use of the MagLev device to perform separation and then measure the densities of its constituents of the mixture (Figure 9). Because glass and copper are more dense than typical organic materials, an aqueous solution of 3 M $DyCl_3$ was used to levitate these samples.

$DyCl_3$ is a suitable paramagnetic salt for this application because it (i) has a higher magnetic susceptibility than those of more commonly used paramagnetic species (e.g., $MnCl_2$ and $GdCl_3$),[18] (ii) has a high solubility in water (~3.5 M),[18] (iii) is highly transparent (it has a faint yellow color even at high concentrations), (iv) has a low toxicity,[26] and (v) is commercially available at an affordable price. (We purchased 100 g for ~$46.) The mixture was suspended in a $DyCl_3$ solution with 1 wt % Tween-20, and yielded, in the MagLev device, two clearly separated clusters of particles with easily distinguishing colors (Figure 9B). We calculated the densities of the two clusters using eq 2, instead of establishing and using a calibration curve (because there were no easily accessible density standards for this range of density). We calculated, using the eq 2, the profile of $B_z(dB_z/dz)$ along the z-axis over the linear range (e.g., using the calibration curve in Figure 7 for that tube), and then experimentally measured the density (1.6927 g/cm^3 using a densitometer) of the suspending medium (3 M $DyCl_3$), and also its magnetic susceptibility (1.56×10^{-3}, see the Supporting Information for details). We estimated the densities of the copper clusters in individual tubes (see the Supporting Information for details), and then obtained

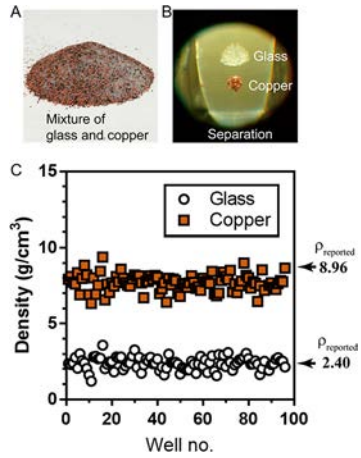

Figure 9. Separation and density measurements of glass particles and copper powder using MagLev (A,B) We mixed fine glass particles (150−212 μm) and copper powder (~420 μm), and separated the mixture into two subpopulations in an aqueous solution of 3 M $DyCl_3$ using MagLev. (C) We estimated the densities of the two subpopulations. The calculated density of the copper cluster is 7.7 ± 0.6 g/cm^3 (N = 95 wells), and the calculated density of the glass cluster is 2.4 ± 0.4 g/cm^3 (N = 95 wells). Literature values ($\rho_{reported}$ = 8.96 g/cm^3 for copper, and $\rho_{reported}$ = 2.40 g/cm^3 for glass) were included for comparison.

an average density of 7.7 ± 0.6 g/cm^3 (N = 95 wells). The estimated average agrees qualitatively ($\Delta\rho$ is 1.3 g/cm^3 or ~14%) with the reported value, 8.96 g/cm^3.[25] This discrepancy may arise from sample preparations (e.g., incomplete removal of trapped air bubbles), and we did not improve the protocol further in this study. We performed similar calculations for the clusters of the glass beads, and obtained an average density of 2.5 ± 0.5 g/cm^3 (N = 95 wells), which agrees with the value, 2.40 ± 0.04 g/cm^3, for the same type of glass beads we measured in a separate study using tilted MagLev.[15]

Density Measurements of Erythrocytes. Erythrocytes served as an example to demonstrate the use of the device to levitate and measure densities of biological particles (Figure 10). In this demonstration, the biocompatible paramagnetic chelate, gadobutrol, was used to levitate erythrocytes. Density

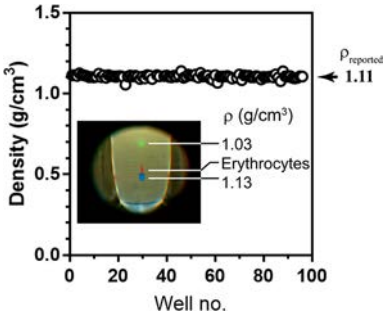

Figure 10. Density measurements of erythrocytes. We levitated diluted whole blood (2000× dilution) in phosphate-buffered saline containing 60.0 mM gadobutrol. We included density standards (the same particles we described in Figure 6) in the same solution to serve as a calibration, and the physical range between the colored particles located within the approximately linear region as validated in Figure 7. The estimated mean density of this sample of erythrocytes is 1.10 ± 0.03 g/cm^3 (N = 93 wells). The literature value ($\rho_{reported}$ = 1.11 g/cm^3) was included for comparison.

DOI: 10.1021/jacs.8b01283
J. Am. Chem. Soc. 2018, 140, 7510−7518

standards (the same particles as we described in Figure 6) were included in the same suspending medium to calibrate the system, and thus to calculate the density of the erythrocyte cluster that located between the two standard particles. No surfactant Tween-20 was used in this experiment (we washed the beads with PBS); enough beads were used so that the majority of the wells had both types of particles that levitated in the medium. (These hydrophobic beads tend to trap at the liquid−air interface in the absence of a surfactant, and we did not optimize the experimental protocol further in this study.) We estimated the density of the erythrocytes to be 1.10 ± 0.03 g/cm^3 (N = 93 wells), which agrees well with the values (~1.11 g/cm^3) reported in the literature.[2,3]

Determination of the Arrhenius Activation Energy of a Reaction on a Solid Support. As the final demonstration, we used the MagLev device to monitor the progress of a coupling reaction of 2,5-diiodobenzoic acid with leucine-functionalized Wang resin (porous polymer beads, 74−149 μm in diameter). MagLev, as we have demonstrated previously using the "standard", single-sample configuration,[27] is a particularly suitable tool with which to monitor conveniently certain types of chemical reactions on solid supports. The coupling reactions, as described in this study, were carried out in a small volume (5 mL) under controlled temperatures (23.6, 7.6, −0.4, and −13.0 °C, see the Supporting Information about the specific cooling baths). Small aliquots (0.5 mL) were sampled periodically during the reaction.

We determined empirically the composition of the suspension medium (11 mM $GdCl_3$ and 0.7 M $ZnBr_2$ in dimethylformamide) to levitate the polymer beads in the device at room temperature (23 ± 1 °C), such that the densities of the unreacted (1.04 g/cm^3, experimentally determined using the "standard" MagLev) and fully converted (1.12 g/cm^3) beads spanned approximately the full linear range of density (Figure 11B). The levitation height of the beads enabled the calculation of the fraction of conversion of the amine present on the beads, and also of the rate constants at different temperatures (Figure 11C, see Supporting Information for details on calculation). We determined the Arrhenius activation of this reaction (Figure 11D) to be 55 kJ/mol, which agrees with a reported value (64 kJ/mol, a relative difference of 14%).[28]

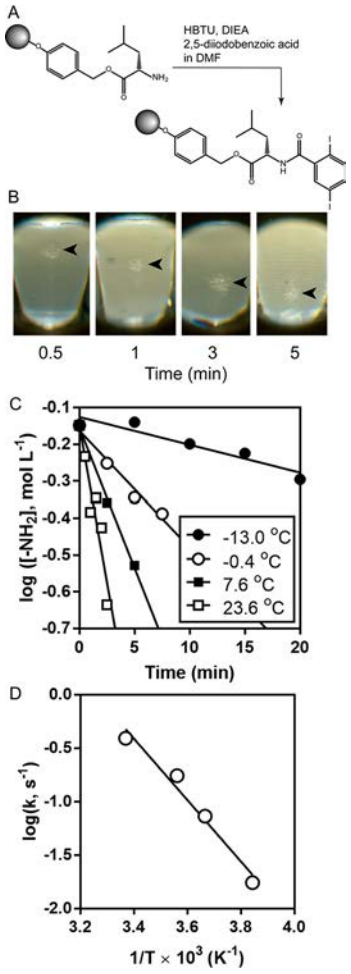

Figure 11. Determination of the Arrhenius activation energy for the coupling reaction of 2,5-diiodobenzoic acid with leucine-functionalized Wang resin. (A) Scheme of the reaction. The reaction was carried out in dimethylformamide (DMF) in the presence of *O*-(benzotriazol-1-yl)-*N*,*N*,*N*′,*N*′-tetramethyluronium hexafluorophosphate (HBTU) and *N*,*N*-diethylisopropylamine (DIEA). (B) MagLev to monitor the progress of the coupling reaction. The levitation height of the beads (marked by the black arrowhead, sampled from the reacting mixture at 23.6 °C at four time points during the reaction) decreased as the reaction proceeded. The suspension medium is DMF containing 11 mM $GdCl_3$ and 0.7 M $ZnBr_2$, and all density measurements were carried out at room temperature (23.6 °C). (C) Unreacted amine present on the resin decreased at different rates over time for reactions carried out at different temperatures. (D) Arrhenius plot to determine the activation energy of this reaction. N = 1 for all measurements.

CONCLUSION

MagLev, as we and others have developed it, is an easily accessible technique with which to separate and measure densities of diamagnetic materials using a paramagnetic suspending medium and inexpensive permanent magnets. The existing methods of MagLev, however, lack a significant analytical capability—high-throughput separation, analysis, and/or density measurements of materials—and this limitation has slowed the development of this technique.

This paper describes the design of a re-engineered configuration that combines the simplicity of MagLev with a broadly available imaging system (a flatbed scanner and simple optics) to levitate and image samples in a paramagnetic medium using 96-well plates. This integrated analytical system delivers the capability of high-throughput analysis in a format that is simple, inexpensive, and broadly applicable to a variety of types of samples—including biological cells—having a size in the range of μm to sub-mm (e.g., particles, powders, emulsions, and living cells). The limitations of the technique are (i) its incompatibility with samples having a size of mm or above and (ii) the use of plastic 96-well plates, which excludes the uses of suspending media that may dissolve the materials of the plates (e.g., polypropylene or polystyrene).

This integrated analytical system is broadly applicable to areas in which density could be exploited as a useful physical parameter, and in which there are needs for simplicity, affordability, and, particularly, the capability to monitor densities of samples in a high-throughput format. This system will broaden density-based applications available to MagLev; it may be particularly useful to (i) materials chemistry to separate, analyze, and/or identify materials, and to monitor physical and/or chemical changes of materials over time,[4] (ii) forensic science and other areas that deal extensively with various sorts of materials (e.g., analysis of trace evidence, and separation/identification of small minerals for geological applications), (iii)

DOI: 10.1021/jacs.8b01283
J. Am. Chem. Soc. 2018, 140, 7510−7518

analytical science to develop broadly useful and easily accessible density-based assays,[23,29] and (iv) biological and medical fields to measure and monitor changes in density associated with cellular activities and/or physiological conditions.[6,8] The optical system and design used may also be valuable for other parallel measurements using similar formats.

■ ASSOCIATED CONTENT

Supporting Information

The Supporting Information is available free of charge on the ACS Publications website at DOI: 10.1021/jacs.8b01283.

Selection of the number and dimensions of magnets; design of an apparatus to image samples that levitate in a 96-well plate using a scanner; assembly of the device; analysis of images; estimation of experimental uncertainty; determination of the magnetic susceptibility of a paramagnetic medium; experimental procedures to perform the coupling reaction of 2,5-diiodobenzoic acid with leucine-functionalized Wang resin; and determination of the Arrhenius activation energy of a reaction on a solid support (PDF)

■ AUTHOR INFORMATION

Corresponding Author

*gwhitesides@gmwgroup.harvard.edu

ORCID

George M. Whitesides: 0000-0001-9451-2442

Notes

The authors declare no competing financial interest.

■ ACKNOWLEDGMENTS

This work was funded by the U.S. Department of Energy, Office of Basic Energy Sciences, Division of Materials Sciences and Engineering under Award Number ER45852. Specifically, the DOE grant supported the design of the MagLev device and its use to perform density measurements. S.G. and D.J.P. acknowledge salary support from DOE (Award Number ER45852). Y. Wang and N. Deshler thank the NSF-supported REU program (Grant number: DMR-1420570) for support.

■ REFERENCES

(1) Thanki, P. N.; Ramesh, C.; Singh, R. P. *Polymer* **2001**, *42*, 535−538.

(2) Fabry, M. E.; Mears, J. G.; Patel, P.; Schaefer-Rego, K.; Carmichael, L. D.; Martinez, G.; Nagel, R. L. *Blood* **1984**, *64*, 1042−1046.

(3) Durmus, N. G.; Tekin, H. C.; Guven, S.; Sridhar, K.; Arslan Yildiz, A.; Calibasi, G.; Ghiran, I.; Davis, R. W.; Steinmetz, L. M.; Demirci, U. *Proc. Natl. Acad. Sci. U. S. A.* **2015**, *112*, E3661−3668.

(4) Ge, S.; Semenov, S. N.; Nagarkar, A. A.; Milette, J.; Christodouleas, D. C.; Yuan, L.; Whitesides, G. M. *J. Am. Chem. Soc.* **2017**, *139*, 18688−18697.

(5) Eren, H. in *The Measurement, Instrumentation, and Sensors Handbook*; Webster, J. G., Ed.; CRC Press, LLC: Boca Raton, FL, 1999.

(6) Grover, W. H.; Bryan, A. K.; Diez-Silva, M.; Suresh, S.; Higgins, J. M.; Manalis, S. R. *Proc. Natl. Acad. Sci. U. S. A.* **2011**, *108*, 10992−10996.

(7) Mace, C. R.; Akbulut, O.; Kumar, A. A.; Shapiro, N. D.; Derda, R.; Patton, M. R.; Whitesides, G. M. *J. Am. Chem. Soc.* **2012**, *134*, 9094−9097.

(8) Kumar, A. A.; Patton, M. R.; Hennek, J. W.; Lee, S. Y.; D'Alesio-Spina, G.; Yang, X.; Kanter, J.; Shevkoplyas, S. S.; Brugnara, C.; Whitesides, G. M. *Proc. Natl. Acad. Sci. U. S. A.* **2014**, *111*, 14864−14869.

(9) Mirica, K. A.; Shevkoplyas, S. S.; Phillips, S. T.; Gupta, M.; Whitesides, G. M. *J. Am. Chem. Soc.* **2009**, *131*, 10049−10058.

(10) Xia, N.; Zhao, P.; Xie, J.; Zhang, C. Q.; Fu, J. Z. *Polym. Test.* **2017**, *63*, 455−461.

(11) Tasoglu, S.; Yu, C. H.; Liaudanskaya, V.; Guven, S.; Migliaresi, C.; Demirci, U. *Adv. Healthcare Mater.* **2015**, *4*, 1469−1476.

(12) Lara, O.; Tong, X.; Zborowski, M.; Chalmers, J. J. *Exp. Hematol.* **2004**, *32*, 891−904.

(13) McCloskey, K. E.; Chalmers, J. J.; Zborowski, M. *Anal. Chem.* **2003**, *75*, 6868−6874.

(14) Sun, L.; Zborowski, M.; Moore, L. R.; Chalmers, J. J. *Cytometry* **1998**, *33*, 469−475.

(15) Nemiroski, A.; Soh, S.; Kwok, S. W.; Yu, H. D.; Whitesides, G. M. *J. Am. Chem. Soc.* **2016**, *138*, 1252−1257.

(16) Nemiroski, A.; Kumar, A. A.; Soh, S.; Harburg, D. V.; Yu, H. D.; Whitesides, G. M. *Anal. Chem.* **2016**, *88*, 2666−2674.

(17) Knowlton, S. M.; Sencan, I.; Aytar, Y.; Khoory, J.; Heeney, M. M.; Ghiran, I. C.; Tasoglu, S. *Sci. Rep.* **2015**, *5*, 15022.

(18) Pulko, B.; Yang, X.; Lei, Z.; Odenbach, S.; Eckert, K. *Appl. Phys. Lett.* **2014**, *105*, 232407.

(19) Cugat, O.; Delamare, J.; Reyne, G. *IEEE Trans. Magn.* **2003**, *39*, 3607−3612.

(20) Bwambok, D. K.; Thuo, M. M.; Atkinson, M. B.; Mirica, K. A.; Shapiro, N. D.; Whitesides, G. M. *Anal. Chem.* **2013**, *85*, 8442−8447.

(21) Mirica, K. A.; Phillips, S. T.; Mace, C. R.; Whitesides, G. M. *J. Agric. Food Chem.* **2010**, *58*, 6565−6569.

(22) Winkleman, A.; Gudiksen, K. L.; Ryan, D.; Whitesides, G. M.; Greenfield, D.; Prentiss, M. *Appl. Phys. Lett.* **2004**, *85*, 2411−2413.

(23) Andersen, M. S.; Howard, E.; Lu, S.; Richard, M.; Gregory, M.; Ogembo, G.; Mazor, O.; Gorelik, P.; Shapiro, N. I.; Sharda, A. V.; Ghiran, I. *Lab Chip* **2017**, *17*, 3462−3473.

(24) Bloxham, W. H.; Hennek, J. W.; Kumar, A. A.; Whitesides, G. M. *Anal. Chem.* **2015**, *87*, 7485−7491.

(25) *CRC Handbook of Chemistry and Physics*, 98th ed.; Rumble, J. R., Ed.; CRC Press: Boca Raton, FL, 2017−2018.

(26) Nakamura, Y.; Tsumura, Y.; Tonogai, Y.; Shibata, T.; Ito, Y. *Toxicol. Sci.* **1997**, *37*, 106−116.

(27) Mirica, K. A.; Phillips, S. T.; Shevkoplyas, S. S.; Whitesides, G. M. *J. Am. Chem. Soc.* **2008**, *130*, 17678−17680.

(28) Benz, L.; Cesafsky, K. E.; Le, T.; Park, A.; Malicky, D. *J. Chem. Educ.* **2012**, *89*, 776−779.

(29) Shapiro, N. D.; Mirica, K. A.; Soh, S.; Phillips, S. T.; Taran, O.; Mace, C. R.; Shevkoplyas, S. S.; Whitesides, G. M. *J. Am. Chem. Soc.* **2012**, *134*, 5637−5646.

DOI: 10.1021/jacs.8b01283
J. Am. Chem. Soc. 2018, 140, 7510−7518